Nonunitarity of the lepton mixing matrix at the European Spallation Source

Sabya Sachi Chatterjee[1,2,*] O. G. Miranda[3,†] M. Tórtola[4,5,‡] and J. W. F. Valle[5,§]

[1]*Institut de Physique Théorique, Université Paris Saclay, CNRS, CEA, F-91191 Gif-sur-Yvette, France*
[2]*Institute for Particle Physics Phenomenology, Department of Physics, Durham University,*
Durham DH1 3LE, United Kingdom
[3]*Departamento de Física, Centro de Investigación y de Estudios Avanzados del IPN,*
Apartado Postal 14-740 07000 Mexico, Distrito Federal, Mexico
[4]*Departament de Física Teórica, Universitat de València, Burjassot 46100, Spain*
[5]*AHEP Group, Institut de Física Corpuscular—CSIC/Universitat de València, Parc Científic de Paterna.*
C/ Catedrático José Beltrán, 2 E-46980 Paterna (Valencia), Spain

If neutrinos get mass through the exchange of lepton mediators, as in seesaw schemes, the neutrino appearance probabilities in oscillation experiments are modified due to effective nonunitarity of the lepton mixing matrix. This also leads to new *CP* phases and an ambiguity in underpinning the "conventional" phase of the three-neutrino paradigm. We study the *CP* sensitivities of various setups based at the European Spallation Source neutrino super-beam (ESSnuSB) experiment in the presence of nonunitarity. We also examine its potential in constraining the associated new physics parameters. Moreover, we show how the combination of DUNE and ESSnuSB can help further improve the sensitivities on the nonunitarity parameters.

I. INTRODUCTION

The discovery of neutrino oscillations [1,2] has brought neutrinos to the center of particle physics. The current experimental data mainly converge into a consistent global picture in which the oscillation parameters are pretty well determined. However, three challenges still remain, namely, to determine the *CP* phase, the atmospheric octant, and the ordering of the neutrino mass spectrum [3,4]. These will be the target of a number of future experiments, such as DUNE [5]. A fourth item must be added to this list, namely, probing the robustness of the interpretation, such as testing the unitarity of the lepton mixing matrix. This is crucial because it undermines the efforts of underpinning the *CP* phase δ_{CP} [6,7].

This task is well justified also on theory grounds. Indeed, one of the most attractive ways to generate neutrino mass is through the mediation of heavy neutral leptons. While these emerge in many gauge extensions of the Standard Model

(SM), they can be postulated directly at the $\mathrm{SU(3)_c} \otimes \mathrm{SU(2)_L} \otimes \mathrm{U(1)_Y}$ level, as the neutrino mass generation mediators.

This, in fact, provides the most general realization of the seesaw mechanism and many of its variants [8]. For generality here we focus exclusively on this case, namely, the standard $\mathrm{SU(3)_c} \otimes \mathrm{SU(2)_L} \otimes \mathrm{U(1)_Y}$ seesaw mechanism. The resulting lepton mixing matrix is, in general, quite complex when compared with Cabibbo—Kobayashi—Maskawa (CKM) mixing. First, lepton mixing contains extra phases that cannot be eliminated by field redefinitions [8] and are therefore physical [9], crucially affecting lepton number violating processes. However, they do not affect conventional oscillations, so we will ignore them in what follows. On the other hand, the lepton mixing matrix must, in general, take into account the admixture of the heavy lepton seesaw mediators with the light active neutrinos [10]. These are usually neglected, as the smallness of neutrino masses indicated by neutrino experiments suggests a very high seesaw scale.

Nonetheless, the seesaw mechanism can also be realized at low scales. The template for this is a scenario where two SM-singlet leptons are added sequentially, instead of just one. If a lepton number symmetry is imposed, then all three active neutrinos are massless, as in the standard model. In contrast to the Standard Model, however, lepton flavor is violated, and similarly, leptonic *CP* symmetry. This shows that flavor and *CP* violation can exist in the leptonic weak

[*]sabya-sachi.chatterjee@ipht.fr
[†]omr@fis.cinvestav.mx
[‡]mariam@ific.uv.es
[§]valle@ific.uv.es

interaction despite the masslessness of neutrinos, implying that such processes need not be suppressed by the small neutrino masses, and hence can be large [11–16].

Over such a basic template one can build genuine "low-scale" realizations of the seesaw mechanism in which lepton number symmetry is restored at low, instead of high, values of the lepton number violating scale. The models are natural in the t'Hooft sense, and lead to small, symmetry-protected neutrino masses. Such low-scale see-saw realizations include the inverse [17,18] as well as the linear seesaw mechanisms [19–21]. In all of these we expect potentially sizeable unitarity violation in the lep-tonic weak interaction. This paper is dedicated to probing such effects at the European Spallation Source neutrino Super-Beam (ESSnuSB) experiment. As far as we can tell, this is the first study of this kind for ESSnuSB. In addition, we also review the sensitivities of the DUNE experiment to the nonunitarity parameters and show how DUNE and ESSnuSB can play complementary roles to each other. Sensitivity studies of nonunitarity at other future neutrino facilities can be found in Refs. [7,22–29].

We briefly describe the theoretical framework for uni-tarity violation in the charged current (CC) leptonic weak interaction in Sec. II, and the matter three-neutrino oscil-lation probabilities with and without unitarity violation in Sec. III. Next, in Sec. IV, we describe the experimental setups of interest, and also present the details of the simulation we have performed. Our results are given in Sec. V and include our calculated ESSnuSB and DUNE sensitivities to nonunitary (NU) neutrino mixing in Sec. V A, the *CP* violation discovery potential in the presence of unitarity violation is given in V B, and the *CP* reconstruction capabilities both for the standard phase as well as the seesaw phase of α_{21} in V C. Finally, we briefly summarize in Sec. VI.

II. THEORETICAL FRAMEWORK

In the standard 3×3 oscillation picture, the neutrino mixing matrix is described symmetrically by a product of three mixing matrices

$$U = \omega_{23}\, \omega_{13}\, \omega_{12}, \tag{1}$$

where each $\omega_{i,j}$ describes an effective 2×2 complex rotation, characterized by a mixing angle and its phase. This symmetrical form complements the original descrip-tion [8] by specifying the most convenient factor ordering. In explicit form, the standard 3×3 leptonic mixing matrix is given by

$$U = \begin{pmatrix} 1 & 0 & 0 \\ 0 & c_{23} & e^{-i\varphi_{23}}s_{23} \\ 0 & -e^{i\varphi_{23}}s_{23} & c_{23} \end{pmatrix} \begin{pmatrix} c_{13} & 0 & e^{-i\varphi_{13}}s_{13} \\ 0 & 1 & 0 \\ -e^{i\varphi_{13}}s_{13} & 0 & c_{13} \end{pmatrix} \begin{pmatrix} c_{12} & e^{-i\varphi_{12}}s_{12} & 0 \\ -e^{i\varphi_{12}}s_{12} & c_{12} & 0 \\ 0 & 0 & 1 \end{pmatrix}, \tag{2}$$

where $s_{ij} = \sin\theta_{ij}$, $c_{ij} = \cos\theta_{ij}$, and φ_{ij} is the correspond-ing phase. One sees the appearance of two extra physical phases with no counterpart in the quark sector: the so-called Majorana phases [8]. Note that the above parametrization of the neutrino mixing matrix is equivalent to the oscil-lation-sensitive part of the PDG form [30] with $\varphi_{13} - \varphi_{12} - \varphi_{23} \equiv \delta_{\mathrm{CP}}$ [31] so that when $\varphi_{12} = \varphi_{23} = 0$ one has $\varphi_{13} = \delta_{\mathrm{CP}}$.

Apart from the presence of these new physical [9] phases, the leptonic CC interaction will, in general, also contain the mixing of neutral heavy leptons that mediate neutrino mass generation, as in the so-called type-I seesaw mechanism. These two facts make the mixing of massive neutrinos substantially richer in structure than that which describes the quark weak interactions [8]. As a result, in this general neutrino framework, $U^{n \times n}$ can be expressed as the product of the new physics (NP) piece times the SM piece

$$U^{n \times n} = U^{\mathrm{NP}} U^{\mathrm{SM}}. \tag{3}$$

Thinking in terms of the seesaw mechanism, it is conven-ient to express the full U matrix as four submatrices. Here we label them as in [32],[1] i.e.,

$$U^{n \times n} = \begin{pmatrix} N & S \\ T & V \end{pmatrix}. \tag{4}$$

Notice that we have a block, N, relating the light neutrino sector with the three active neutrino flavors. Here V will be a $(n-3) \times (n-3)$ submatrix, while S and T will be, in general, rectangular matrices.

Clearly, in this general case, the full unitarity condition will take the form

$$NN^\dagger + SS^\dagger = I,$$
$$TT^\dagger + VV^\dagger = I. \tag{5}$$

---

[1]The form of the matrices N, S, T, and V within the full seesaw expansion was given in Ref. [10]. They correspond, respectively, to U_a, U_b, U_c and U_d of Eqs. (2.8) and (3.5) of the above reference.

Therefore, the 3×3 matrix N describing the mixing of light neutrinos will no longer be unitary. One can show [33] that in the most general case N can be parametrized as

$$N = N^{NP}U^{3\times3} = \begin{pmatrix} \alpha_{11} & 0 & 0 \\ \alpha_{21} & \alpha_{22} & 0 \\ \alpha_{31} & \alpha_{32} & \alpha_{33} \end{pmatrix} U^{3\times3}, \quad (6)$$

where the diagonal α's are real and close to 1, while the off diagonals are small but complex. Indeed, for any number of additional neutrino states, we will have for the diagonal entries of this matrix that

$$\alpha_{jj} := \prod_{i=4,n} \cos\theta_{ji}, \quad (7)$$

with no sum over j. For small mixings, the nondiagonal entries are given as

$$\alpha_{ji} \simeq -\sum_{k=4,n} \theta_{jk}\theta_{ik}e^{-i(\varphi_{jk}-\varphi_{ik})}; \quad i < j. \quad (8)$$

From this last expression, one can see that

$$|\alpha_{21}|^2 \le \sum_{i=4}^{N} |\theta_{2i}\theta_{1i}e^{-i(\varphi_{2i}-\varphi_{1i})}|^2 = \sum_{i=4}^{N} \theta_{2i}^2\theta_{1i}^2, \quad (9)$$

and similar equations for the other two nondiagonal terms. Using the triangle inequality, one can now derive the consistency relations,[2]

$$|\alpha_{ji}| \le \sqrt{(1-\alpha_{jj}^2)(1-\alpha_{ii}^2)}. \quad (10)$$

The muon neutrino appearance probability will be given as

$$P_{\mu e} = \alpha_{11}^2|\alpha_{21}|^2 - 4\sum_{j>i}^{3} \text{Re}\,[N_{\mu j}^*N_{ej}N_{\mu i}N_{ei}^*]\sin^2\left(\frac{\Delta m_{ji}^2 L}{4E}\right)$$

$$+ 2\sum_{j>i}^{3} \text{Im}\,[N_{\mu j}^*N_{ej}N_{\mu i}N_{ei}^*]\sin\left(\frac{\Delta m_{ji}^2 L}{2E}\right), \quad (11)$$

where N is given in terms of the α's as in Eq. (6).

For the case of vacuum oscillations, the parameters characterizing unitarity violation in the $\mu - e$ sector are α_{11}, α_{22}, and α_{21}. In the presence of matter effects, the appearance probability could also involve the third neutrino type, since the charged and neutral current potential will modify the effective form of the matrix N. The charged current potential for the nonunitary case will be given by

---

$$V_{CC}^{\alpha\beta} = \sqrt{2}G_F N_e (NN^\dagger)_{\alpha e}(NN^\dagger)_{e\beta}, \quad (12)$$

where G_F is the Fermi constant and N_e the number density of electrons in the medium. The matrix product will be written, in terms of the α's, as [7]

$$(NN^\dagger)_{\alpha e}(NN^\dagger)_{e\beta} = \alpha_{11}^2 \begin{pmatrix} \alpha_{11}^2 & \alpha_{11}\alpha_{21}^* & \alpha_{11}\alpha_{31}^* \\ \alpha_{11}\alpha_{21} & |\alpha_{21}|^2 & \alpha_{21}\alpha_{31}^* \\ \alpha_{11}\alpha_{31} & \alpha_{21}^*\alpha_{31} & |\alpha_{31}|^2 \end{pmatrix}. \quad (13)$$

The corresponding potential for neutral currents will be

$$V_{NC}^{\alpha\beta} = -\sqrt{2}G_F\frac{N_n}{2}\sum_\rho (NN^\dagger)_{\alpha\rho}(NN^\dagger)_{\rho\beta}$$

$$= -\sqrt{2}G_F\frac{N_n}{2}[(NN^\dagger)^2]_{\alpha\beta}, \quad (14)$$

where the matrix product $(NN^\dagger)^2$, at leading order in the nondiagonal α's, takes the form [7]

$$\begin{pmatrix} \alpha_{11}^4 & \alpha_{11}\alpha_{21}^*(\alpha_{11}^2+\alpha_{22}^2) & \alpha_{11}\alpha_{31}^*(\alpha_{11}^2+\alpha_{33}^2) \\ \alpha_{11}\alpha_{21}(\alpha_{11}^2+\alpha_{22}^2) & \alpha_{22}^4 & \alpha_{22}\alpha_{32}^*(\alpha_{22}^2+\alpha_{33}^2) \\ \alpha_{11}\alpha_{31}(\alpha_{11}^2+\alpha_{33}^2) & \alpha_{22}\alpha_{32}(\alpha_{22}^2+\alpha_{33}^2) & \alpha_{33}^4 \end{pmatrix}. \quad (15)$$

Neglecting cubic terms in α_{21}, $\sin\theta_{13}$, and Δm_{21}^2, one finds that, in the vacuum case limit, the main contribution to the conversion probability will be given by

$$P_{\mu e} = (\alpha_{11}\alpha_{22})^2 P_{\mu e}^{3\times3} + \alpha_{11}^2\alpha_{22}|\alpha_{21}|P_{\mu e}^I + \alpha_{11}^2|\alpha_{21}|^2, \quad (16)$$

where $P_{\mu e}^{3\times3}$ denotes the usual three-neutrino conversion probability,

$$P_{\mu e}^{3\times3} = 4\left[\cos^2\theta_{12}\cos^2\theta_{23}\sin^2\theta_{12}\sin^2\left(\frac{\Delta m_{21}^2 L}{4E_\nu}\right)\right.$$

$$\left. + \cos^2\theta_{13}\sin^2\theta_{13}\sin^2\theta_{23}\sin^2\left(\frac{\Delta m_{31}^2 L}{4E_\nu}\right)\right]$$

$$+ \sin 2\theta_{12}\sin\theta_{13}\sin 2\theta_{23}\sin\left(\frac{\Delta m_{21}^2 L}{2E_\nu}\right)$$

$$\times \sin\left(\frac{\Delta m_{31}^2 L}{4E_\nu}\right)\cos\left(\frac{\Delta m_{31}^2 L}{4E_\nu} + \delta_{CP}\right), \quad (17)$$

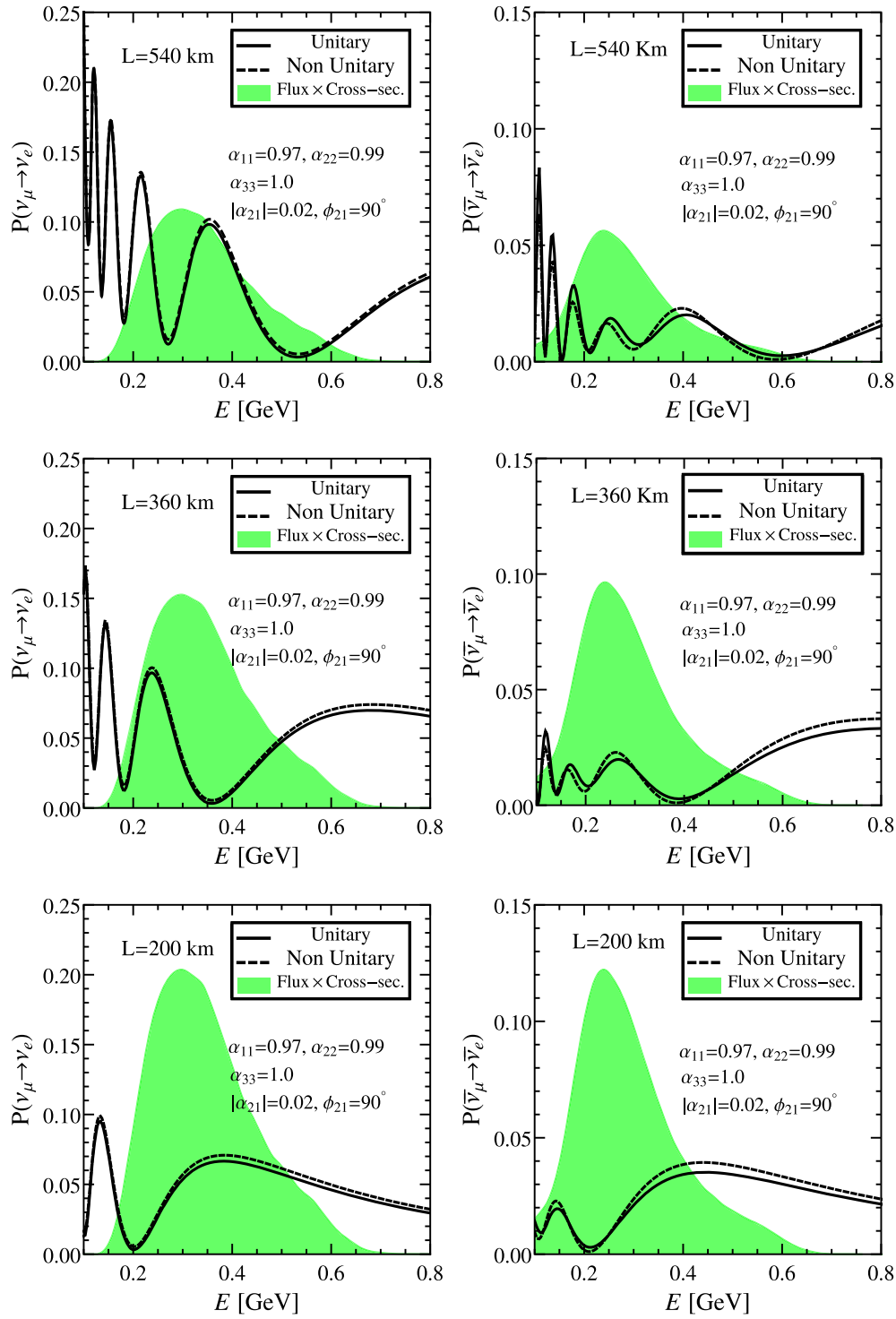where $P_{\mu e}^I$ is the interference term

FIG. 1. The left panels represent the neutrino appearance probabilities for the unitary (solid line) and nonunitary (dashed line) oscillation cases, for three different baselines, as indicated. The right panels show the corresponding antineutrino probabilities. The product of the $\nu_\mu (\bar{\nu}_\mu)$ fluxes and the $\nu_e (\bar{\nu}_e)$-nucleus cross sections (in arbitrary units) is also shown as a green shaded area.

$$P^I_{\mu e} = -2\left[\sin(2\theta_{13})\sin\theta_{23}\sin\left(\frac{\Delta m^2_{31}L}{4E_\nu}\right)\sin\left(\frac{\Delta m^2_{31}L}{4E_\nu} + \delta_{CP} - \phi_{21}\right)\right] + \cos\theta_{13}\cos\theta_{23}\sin 2\theta_{12}\sin\phi_{21}\sin\left(\frac{\Delta m^2_{21}L}{2E_\nu}\right),$$

(18)

with $\phi_{21} = \arg(\alpha_{21})$.

TABLE I.   Benchmark values for the standard three-neutrino oscillation parameters taken from the current global fit analysis [3], along with their assumed marginalization status within our analyses, except δ_{CP}. For simplicity, normal mass ordering (NO) has been assumed.

3ν Parameters	$\sin^2\theta_{12}$	$\sin^2\theta_{13}$	$\sin^2\theta_{23}$	δ_{CP}	$\frac{\Delta m_{21}^2}{10^{-5}\text{eV}^2}$	$\frac{\Delta m_{31}^2}{10^{-3}\text{eV}^2}$
Benchmark values	0.318	0.022	0.57	$[-180, 180]$	7.5	2.55
Status	Fixed	Marginalized	Marginalized	Marginalized	Fixed	Marginalized

III. THREE-NEUTRINO OSCILLATION PROBABILITIES

Before coming to our numerical results, in this section we discuss the behavior of the appearance (anti)neutrino probabilities. To this end, we show in the left (right) panel of Fig. 1 the $\nu_\mu \to \nu_e$ ($\bar{\nu}_\mu \to \bar{\nu}_e$) oscillation probabilities as a function of the neutrino energy. The upper, middle, and lower panels correspond to 540, 360, and 200 km baselines, respectively. We show the conversion probability in the standard unitary framework as a solid line, while the dashed one represents the nonunitary case. For the unitary case, we consider the values of the neutrino oscillation parameters given in Table I with $\delta_{CP} = -90°$. For the nonunitary case, besides these values, we fix the nonunitary α parameters to be $\alpha_{11} = 0.97$, $\alpha_{22} = 0.99$, $\alpha_{33} = 1$, $|\alpha_{21}| = 0.02$, $\phi_{21} = 90°$, $|\alpha_{31}| = 0$, and $|\alpha_{32}| = 0$. In Fig. 1 we also include in green color (arbitrary units) the unoscillated (anti)neutrino ν_μ flux times the (anti)ν_e nucleus cross section [35,36]. This provides a bird's-eye view of the real analysis at the event level. The main region of interest extends from 0.1 to 0.7 GeV, with a peak around 0.30 GeV. One can see the relative location of this peak with respect to the second oscillation maximum for the three baselines of 540 and 360 km and the 200 km case; see also Table II. The true expected event number for the appearance signal must, of course, take into account the convolution of the cross section, the appearance probability, and the unoscillated neutrino energy spectrum at the detector, which depends on its distance to the source. Thus, the total unoscillated neutrino flux for the 200 km case will be approximately 3 times that for a 360 km baseline and 7 times the flux of the 540 km case. As a result, the shorter the baseline, the higher the expected number of events, as we will see in Fig. 3.

TABLE II.   Possible baselines of the ESSnuSB project [37–40], along with the corresponding values of the neutrino energy for the first and second oscillation maxima.

Baseline (km)	First oscillation maxima (GeV)	Second oscillation maxima (GeV)
540	1.05	0.35
360	0.70	0.23
200	0.39	0.13

IV. EXPERIMENTAL SETUP AND SIMULATION

In this section, we briefly discuss the experimental specifications of the ESSnuSB and DUNE setups used in this work, followed by a description of our simulation procedure.

A. Experimental setup options

The ESSnuSB project is a proposed accelerator neutrino experiment sourced at Lund (Sweden), where the ESS linac facility is currently under construction. The original ESSnuSB proposal was to use a very intense proton beam of 2 GeV energy and an average beam power of 5 MW, resulting in 2.7×10^{23} protons on target per year (208 effective days) [37–40]. Here we will adopt this configuration. It is expected that the future linac upgrade can increase the proton energy up to 3.6 GeV. The neutrino and antineutrino fluxes arising from the 2 GeV proton beam peak around 0.25 GeV [41]. These (anti)neutrinos will be detected by a 500 kton fiducial mass water Cherenkov detector similar to the MEMPHYS project [42,43]. Since the baseline of the far detector has not been finalized yet, we have considered in this work three possible baselines [37], which are 200, 360, and 540 km respectively. It has been shown in [37] that if the detector is placed in any of the existing mines in between 200 to 600 km from the ESSnuSB site Lund, a 3σ evidence of CP violation could be achieved for 60% coverage of the full δ_{CP} range. Our simulation matches the event numbers of Table 3 and all other results given in [37]. In all the numerical results presented here, we have assumed 2 years of neutrino and 8 years of antineutrino running with an optimistic assumption of uncorrelated 5% signal normalization and 10% background normalization error for both neutrino and antineutrino appearance and disappearance channels, respectively. For more details about the accelerator facility, beamline design, detector, and baseline positions of this setup, see [37]. Note that, while working on this paper, an updated analysis from the collaboration has come out [44].[3] Enhanced sensitivities to unitarity violation might be expected for the updated setup of the proposal. This high potential and ambitious facility is expected to start taking data around the year 2030.

---

[3]Reference [44] has not considered the 200 km baseline option which, as we will see, actually turns out to be somewhat more promising for certain tasks, e.g., probing α_{21}.

TABLE III. Current neutrino constraints on the nonunitary parameters from Ref. [34].

NU Parameters	$|\alpha_{21}|$	$|\alpha_{31}|$	$|\alpha_{32}|$	α_{11}	α_{22}	α_{33}
3σ bounds	<0.025	<0.077	<0.020	>0.929	>0.987	>0.715

DUNE is a future long-baseline accelerator-based neutrino experiment with a baseline of 1300 km from the source at Fermilab to the far detector placed deep underground at the Sanford Laboratory site in South Dakota. DUNE will use a 40 kton LArTPC detector and a 120 GeV proton beam with 1.2 MW beam power resulting in 1.1×10^{21} protons on target per year. For the numerical simulations, we have followed the experimental configurations provided by the collaboration in the Technical Design Report [45,46], assuming an equal runtime of 3.5 years in neutrino and antineutrino modes, which results in a 336 kton-MW-year exposure for the Technical Design Report setup. More details on the systematic errors, efficiencies, and energy resolutions can be found in Refs. [46,47].

B. Simulation procedure

In order to assess the statistical sensitivity of the ESSnuSB facility to neutrino oscillations, we have made use of the built-in χ^2 function of the GLoBES package [48,49], which incorporates the systematic errors through the pull terms [50]. To perform the nonunitarity analysis we have used the modified version of [51]. The total χ^2 is a sum of all the contributions coming from different channels,

$$\chi^2_{\text{total}} = \chi^2_{\nu_\mu \to \nu_e} + \chi^2_{\bar{\nu}_\mu \to \bar{\nu}_e} + \chi^2_{\nu_\mu \to \nu_\mu} + \chi^2_{\bar{\nu}_\mu \to \bar{\nu}_\mu}. \qquad (19)$$

Unless stated otherwise, the benchmark choices of the standard three-neutrino unitary oscillation parameters and

their marginalization status in our analysis are given in Table I. Our benchmark choices closely follow the current global fit analysis [3]. Following the same analysis, we have adopted a 1% uncertainty on the atmospheric mass-squared splitting Δm_{31}^2 and a 3.2% uncertainty on the reactor mixing angle $\sin^2 \theta_{13}$. We have freely marginalized over the atmospheric parameter $\sin^2 \theta_{23}$ from 0.35 to 0.65.

For the case of ESSnuSB, we have considered a line-averaged constant matter density $\rho = 2.8$ g/cm³ following the PREM profile [52,53]. For DUNE, we have also assumed the same matter density but with a 5% uncertainty due to the longer baseline. For definiteness, we have assumed the currently preferred case of normal mass ordering (NO) throughout all of our analyses. Whenever appropriate, we have also marginalized over the NU parameters, along with their associated *CP* phases, implementing the current 3σ bounds shown in Table III. These come essentially from short-baseline oscillation searches such as from NOMAD [54,55] and CHORUS [56,57] and the long-baseline experiments T2K [58], NOvA [59] and, most importantly, MINOS/MINOS+ [60].

V. RESULTS

In this section we discuss in detail the numerical findings of our analyses, where we explore the sensitivity of the ESSnuSB facility to the nonunitary neutrino mixing, as well as the impact of nonunitarity on the measurement of the standard three-neutrino oscillation parameters, with emphasis on the *CP*-violating phase, δ_{CP}.

A. Probing nonunitary neutrino mixing at ESSnuSB

We start our discussion from Fig. 2, where we show the ESSnuSB sensitivity to nonunitarity in the $(|\alpha_{21}|, \delta_{\text{CP}})$ plane. Left, middle, and right panels show the results for 540, 360,
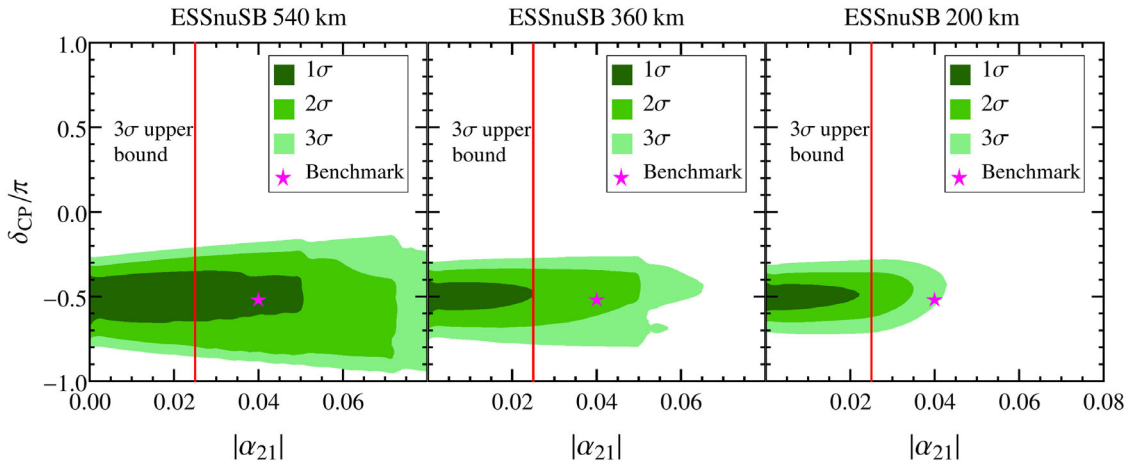

FIG. 2. ESSnuSB sensitivity to the nonunitarity scenario in the $(|\alpha_{21}|, \delta_{\text{CP}})$ plane. Left, middle, and right panels correspond to 540, 360, and 200 km baselines, respectively. Contours are shown at 1σ, 2σ, and 3σ for 2 d.o.f. The red vertical lines indicate the current 3σ upper limit on $|\alpha_{21}|$ from neutrino data. We have assumed $\delta_{\text{CP}}(\text{true}) = -90°$ and normal mass ordering. The magenta star marked as benchmark in each panel has been used later to produce dashed spectra in the upper panel of Fig. 3.
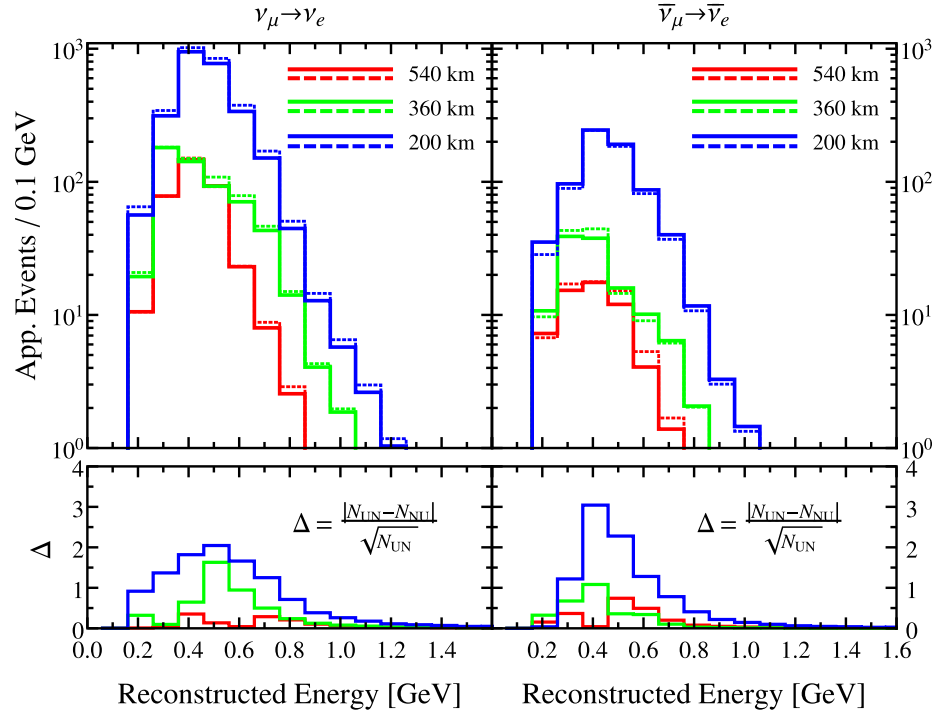
FIG. 3.   Upper panels: $\nu_\mu \rightarrow \nu_e$ and $\bar{\nu}_\mu \rightarrow \bar{\nu}_e$ appearance event spectra as a function of reconstructed neutrino energy at ESSnuSB for different baselines, as indicated. Solid lines represent the standard three-neutrino spectra generated with the standard oscillation parameter values from Table I with $\delta_{\rm CP} = -90°$ and dashed lines correspond to the NU scenario taking the optimized values of the standard oscillation parameters (not shown explicitly) and the new physics nonunitarity parameters from Table IV. The lower panels represent the absolute difference in the appearance events between the UN and the NU scenarios divided by the statistical uncertainty in each bin.

and 200 km baselines, respectively. The light, medium, and dark green contours in each panel correspond to the 1σ, 2σ, and 3σ allowed regions for 2 degrees of freedom (d.o.f.) i.e., $\Delta\chi^2 = 2.3$, 6.18, and 11.83, respectively. In this figure we have assumed the standard unitary framework as the true hypothesis, and then we have fitted the nonunitary hypothesis against it. Normal mass ordering has been assumed all over the analyses. The true data have been generated assuming the benchmark choices of the standard unitary oscillation parameters in Table I with $\delta_{\rm CP}({\rm true}) = -90°$, while for the reconstruction we have fixed the solar oscillation parameters and marginalized over θ_{13}, θ_{23}, and Δm^2_{31}. In addition, we have also marginalized over the NU parameters α_{11}, α_{22}, and α_{33} within their allowed 3σ ranges as given in Table III. We have also freely varied ϕ_{21} from $-\pi$ to $+\pi$. We have assumed zero values of the other nondiagonal NU parameters, $|\alpha_{31}|$ and $|\alpha_{32}|$. The red vertical lines in each panel indicate the current 3σ upper limit on $|\alpha_{21}|$ from neutrino data. One sees that the 200 km baseline gives the best 1σ, 2σ, and 3σ sensitivities on $|\alpha_{21}|$, in comparison to the 360 and 540 km baseline options. Quantitatively, the attainable upper limits for $|\alpha_{21}|$ at 1σ are 0.044, 0.024, and 0.02 for 540, 360, and 200 km baselines, respectively. Conversely, we have checked that there is basically no sensitivity to the new CP phase ϕ_{21} for any of the baselines. On the other hand, the measurement on $\delta_{\rm CP}$ is not affected

much by the presence of nonunitarity. One can also see that the uncertainty on the measurement of $\delta_{\rm CP}$ is the lowest for 200 km and the highest for 540 km.

To understand better the previous result one can select a point allowed at 1σ, 2σ, and 3σ for a 540, 360, and 200 km baselines, respectively. We show in Fig. 3 the appearance event spectra for the neutrino (upper-left panel) and antineutrino (upper-right panel) modes. For each of the three different baselines we choose a benchmark point (magenta star in Fig. 2) given by the NU parameter $|\alpha_{21}| = 0.04$ and the standard CP phase $\delta_{\rm CP} = -90°$. For this benchmark choice, the other NU parameters arising from the χ^2 marginalization take the values shown in Table IV. Note that the optimized values of the standard oscillation parameters are not shown here explicitly. We use all of them as input to generate the event spectra in Fig. 3. These

TABLE IV.   Nonunitarity parameters used for obtaining the nonunitary spectra (dashed line) in Fig. 3; see text for more details.

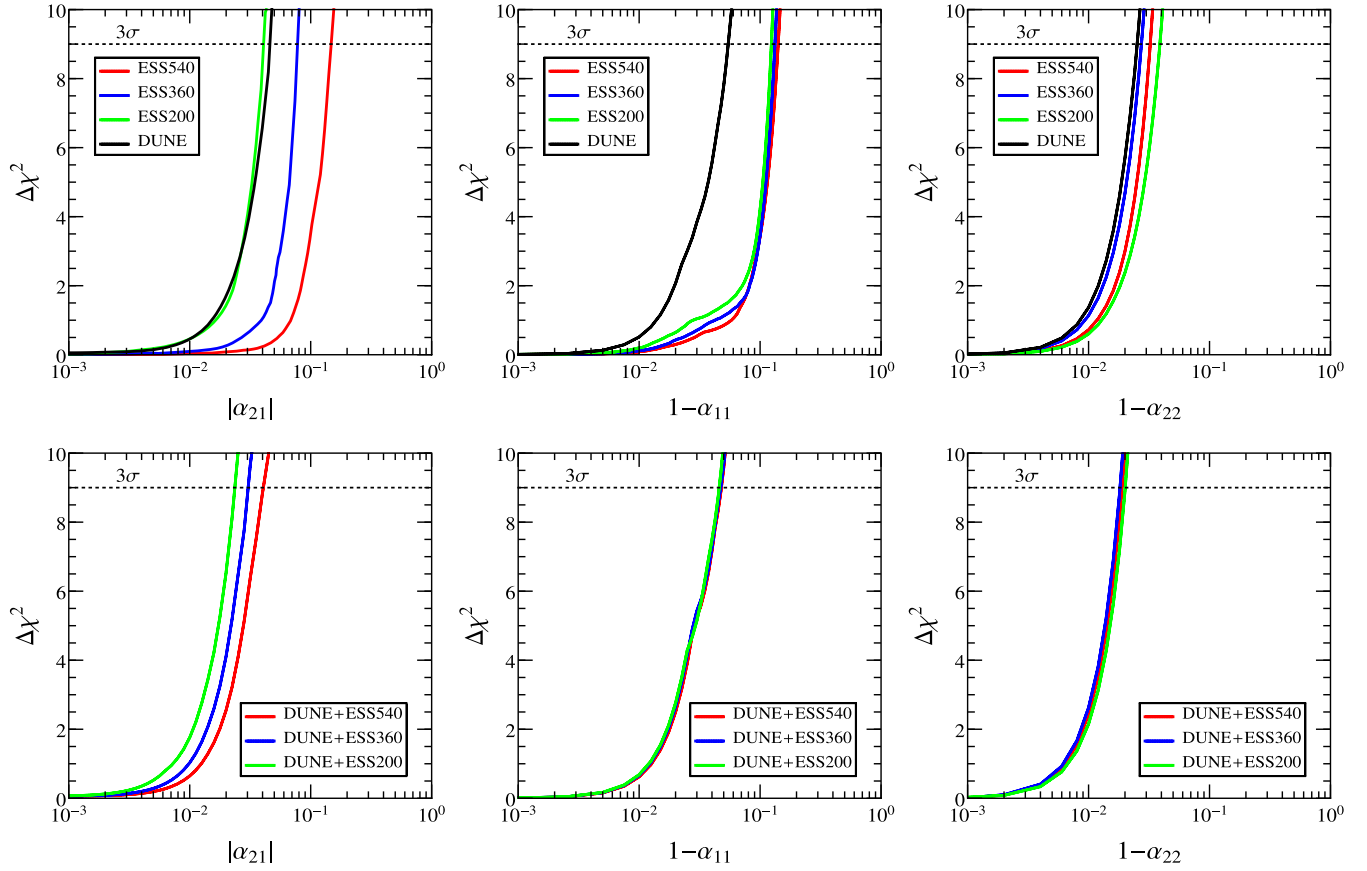| Baseline (km)	α_{11}	α_{22}	α_{33}	ϕ_{21}	$|\alpha_{31}|$	$|\alpha_{32}|$
540	0.95	0.99	0.73	155°	0	0
360	0.94	0.99	0.73	140°	0	0
200	0.94	0.99	0.96	75°	0	0

FIG. 4. Upper panels: One-dimensional $\Delta\chi^2$ projection on the NU parameters $|\alpha_{21}|$ (left), α_{11} (middle), and α_{22} (right panel) for the three different baselines considered for ESSnuSB (red, blue, and green lines, see the legend) and for DUNE (black line). Lower panels: combined sensitivities for DUNE and ESSnuSB for the three baselines considered. Normal mass ordering has been assumed in the analysis.

are shown as dashed lines, while the unitary scenario is represented with solid lines. In order to better compare the standard unitary (UN) with the NU case, we show in the lower panels of Fig. 3 the absolute differences of the number of events divided by the statistical uncertainty in each bin, i.e., $\Delta = |N_{UN} - N_{NU}|/\sqrt{N_{UN}}$. This provides a crude measurement of the statistical significance of our unitarity test. One sees that the best sensitivities to the standard parameter δ_{CP} and the NU parameter $|\alpha_{21}|$ are achieved for the 200 km baseline, as already shown in Fig. 2. Notice also that the 360 km baseline does somewhat better than the 540 km baseline. This is also reflected in the left panels of Fig. 4.

In Fig. 4, we show the one-dimensional projection of the $\Delta\chi^2$ as a function of the NU parameters $|\alpha_{21}|$ (left panel), α_{11} (middle panel), and α_{22} (right panel). The red, blue, and green curves in the upper panels show the sensitivities corresponding to the three ESSnuSB baselines, 540, 360, and 200 km, respectively, while the black curve corresponds to the DUNE sensitivity. In the lower panels, the same color code is used to represent the sensitivities for the combined analysis of DUNE and the ESSnuSB for baselines of 540, 360, and 200 km.

As before, this figure is obtained assuming the standard unitary framework as the true hypothesis, and testing the NU framework against it, i.e., $\Delta\chi^2 = \chi^2_{NU} - \chi^2_{UN}$. The true values of the oscillation parameters are taken from Table I, fixing the two solar parameters θ_{12} and Δm^2_{21} at their benchmark choices, and marginalizing over θ_{13}, θ_{23}, and Δm^2_{31}. Since the exact value of the standard CP phase δ_{CP} is currently not accurately known, we have marginalized over its true and test values within its full range.

For the sensitivity to $|\alpha_{21}|$, shown in the left panels of Fig. 4, we have freely varied the NU parameters α_{11}, α_{22}, and α_{33} within their allowed 3σ ranges as given in Table III and the phase ϕ_{21} from $-\pi$ to $+\pi$. The other nondiagonal NU parameters $|\alpha_{31}|$ and $|\alpha_{32}|$ have been set to zero. From the upper left panel we can see that the best sensitivity for the ESSnuSB comes from the 200 km baseline, followed by the 360 and 540 km baselines. The expected 3σ upper limits on $|\alpha_{21}|$ corresponding to 540, 360, and 200 km baselines are 0.16, 0.075, and 0.04, respectively. These limits would be independent and complementary to those given in Table III and illustrate the ESSnuSB potential in probing new physics. For the case of DUNE, the upper limit at 3σ would be 0.046. One sees the sensitivities

expected at ESSnuSB are competitive and, for the smaller baseline, it performs slightly better than DUNE [7]. In the lower left panel of Fig. 4, we show how the combined sensitivities of DUNE and ESSnuSB, improve with respect to the individual sensitivities. The 3σ upper limits corresponding to the DUNE+ESS540, DUNE+ESS360, and DUNE+ESS200 combinations would be 0.04, 0.03, and 0.022, respectively. It is encouraging to see that the combination of DUNE and the 200 km baseline of ESSnuSB would be able to set a constraint on $|\alpha_{21}|$ which is better than the current 3σ upper bound given in Table III.

The middle panel of Fig. 4 shows the sensitivities to the diagonal NU parameter α_{11}. The analysis method is very similar to the previous one as far as the standard unitarity parameters are concerned. However, for the NU parameters, we marginalize over the parameters α_{22}, $|\alpha_{21}|$, and their associated new CP phase ϕ_{21}. As before, the off-diagonal parameters α_{31} and α_{32} have been set to zero and α_{33} was set to unity. One can see that the 3σ sensitivities on α_{11} corresponding to the 540, 360, and 200 km baselines are lower than for DUNE, i.e., 0.87 versus 0.95. From the lower middle panel one sees that the combined sensitivities corresponding to DUNE+ESS540, DUNE+ESS360, and DUNE+ESS200 are very similar and approximately equal to 0.955, which would somewhat improve the current sensitivity on α_{11}.

The sensitivities on α_{22} are shown in the right panels of Fig. 4. In this case, we follow exactly the same steps as in the α_{11} analysis but marginalizing over α_{11}. Our results show that the best performance is expected from DUNE, followed by the ESSnuSB with baselines 360, 540, and 200 km. The expected sensitivities for the individual setups do not improve over the current lower bound. However, one sees that the combined sensitivity of DUNE and any ESSnuSB baseline gives a slightly lower sensitivity compared to the current 3σ lower bound. One concludes that all these sensitivities, especially those coming from the combined analyses, are encouraging and will play an important role especially when combined with the already available data. For the sake of convenience we quote all our bounds as Table V. Note also that these NU parameter sensitivities at the ESSnuSB may be complemented by additional information coming from future experiments such as T2HK or JUNO [61,62].

TABLE V. ESSnuSB, DUNE, and combined 3σ sensitivities on the NU parameters $|\alpha_{21}|$, α_{11}, and α_{22} obtained in this work.

3σ Sensitivity	$|\alpha_{21}|$	α_{11}	α_{22}
ESS540	<0.160	>0.850	>0.964
ESS360	<0.075	>0.860	>0.973
ESS200	<0.040	>0.870	>0.967
DUNE	<0.046	>0.945	>0.975
DUNE + ESS540	<0.040	>0.951	>0.981
DUNE + ESS360	<0.030	>0.952	>0.982
DUNE + ESS200	<0.022	>0.954	>0.979

B. *CP* violation discovery potential

Now we turn back to the "conventional" CP violation (CPV) discovery potential within our generalized nonunitary framework. The CPV discovery potential of the ESSnuSB and DUNE setup is summarized in Figs. 5, 6, and 7. Our results are given both for the unitary and the nonunitary framework. As in the standard δ_{CP} sensitivity study [5], the CP-violating hypothesis is tested against a CP-conserving scenario through [7]

$$\Delta\chi^2(\delta_{CP}^{\text{true}}) = \text{Min}[\Delta\chi^2(\delta_{CP}^{\text{true}}, \delta_{CP}^{\text{test}} = 0), \Delta\chi^2(\delta_{CP}^{\text{true}}, \delta_{CP}^{\text{test}} = \pm\pi)].$$
(20)

This way, we obtain the significance with which one can reject the test hypothesis of no CP violation. We have assumed five nonzero NU parameters: the three diagonal ones (marginalized over the true and test values), plus one nondiagonal parameter, either $|\alpha_{21}|$ (left panels) or $|\alpha_{31}|$ (right panels), with the associated complex CP phase (ϕ_{21} or ϕ_{31}), also marginalized. Concerning the standard three-neutrino parameters (both in the unitary and nonunitary scenarios), we have marginalized over the two mixing angles θ_{13} and θ_{23} and the "atmospheric" mass-squared splitting Δm_{31}^2. The left (right) column of Fig. 5 represents the CPV discovery potential of ESSnuSB for the three baseline choices and three different values of the NU parameter $|\alpha_{21}|$ ($|\alpha_{31}|$). The black solid line in each plot corresponds to the standard three-neutrino unitary framework. Upper, middle, and lower panels represent the results obtained for 540, 360, and 200 km baselines, respectively. The red, green, and blue dashed curves in the left plots represent the CPV discovery sensitivities in the NU framework corresponding to different values of $|\alpha_{21}|$, 0.01, 0.02, and 0.03, respectively (the latter, relatively large value, is taken mainly for comparison). One sees that the CPV sensitivity in the standard unitary neutrino oscillation framework always lies around 8σ for $\delta_{CP}(\text{true}) = \pm90°$ for all three baselines, see the solid black line in all the panels. This agrees with the results presented in Refs. [37,44,63]. All baselines have more or less similar sensitivities, except for the fact that the δ_{CP} range over which CPV can be established for 540 km and 360 km is slightly bigger than for 200 km. This fact is also confirmed in Ref. [37]. However, we will see the merits of the 200 km baseline in what follows. As far as the NU framework is concerned, two of our benchmark values, $|\alpha_{21}| = 0.01$ and 0.02 lie within the current 3σ limit, whereas $|\alpha_{21}| = 0.03$ lies slightly outside the current allowed limit.[4]

We stress that the CPV discovery sensitivity is degraded with respect to the unitary case. This is expected, due to the

---

[4]As already mentioned, the line with 0.03 is included mainly for comparison, to have a broader view of degrading behavior with respect to the nondiagonal NU parameters.
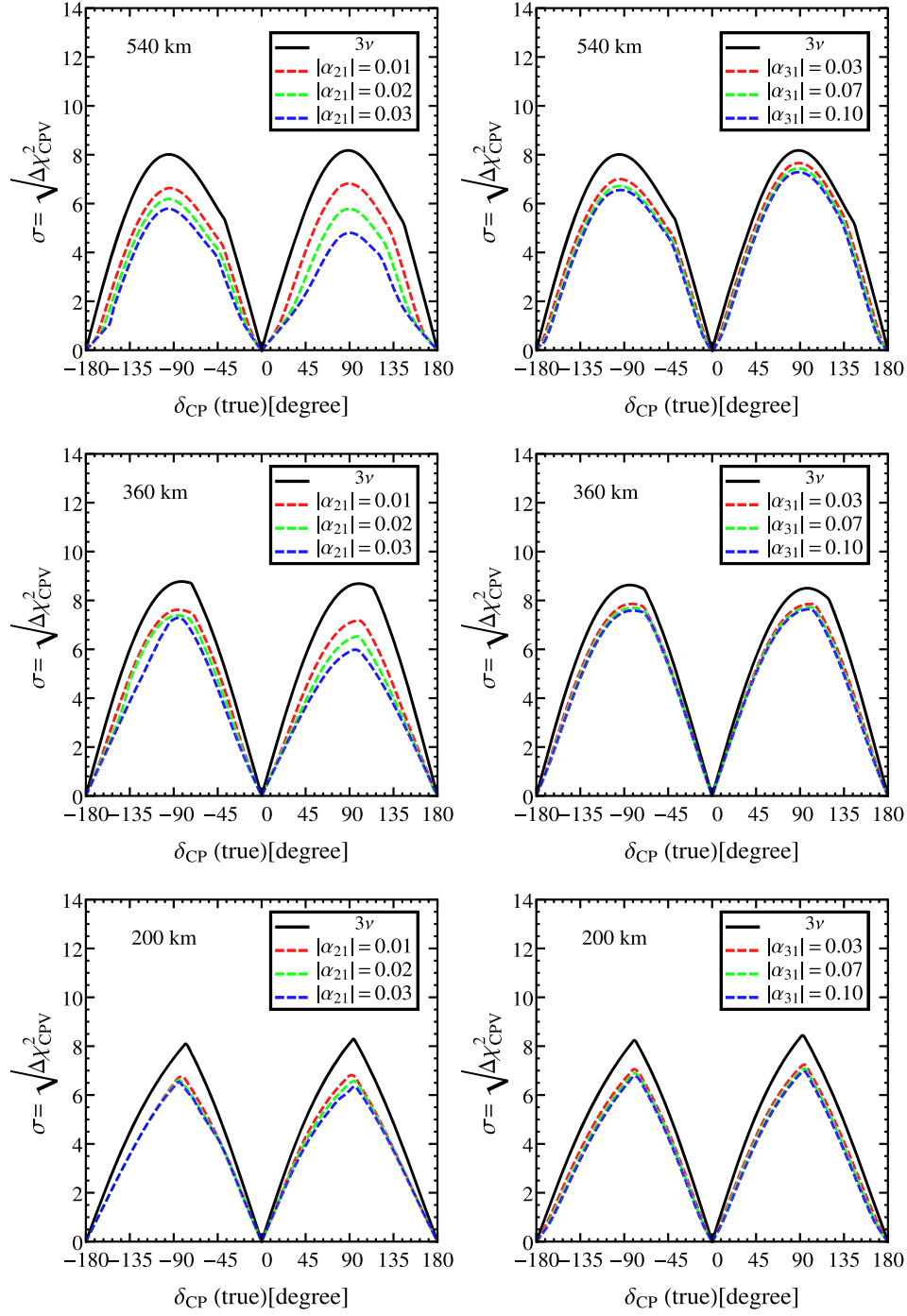
FIG. 5.   CPV sensitivities at ESSnuSB for various baselines, as indicated. The solid black lines correspond to unitary neutrino mixing, while dashed lines show the sensitivities in the presence of unitarity violation. The value of $|\alpha_{21}|$ ($|\alpha_{31}|$) has been fixed in the left (right) panel in the data as well as in the theory. We have marginalized over θ_{13}, θ_{23}, Δm^2_{31}, as well as over the true and test values of α_{11}, α_{22}, α_{33}, and ϕ_{21} (in the left panel) and ϕ_{31} (in the right panel), within their allowed ranges.

presence of new phases associated to unitarity violation [6]. Clearly, the CPV discovery sensitivity decreases with the increasing values of $|\alpha_{21}|$, specially for 540 km, leading to a minimum sensitivity of 4.6σ for $\delta_{CP}(\text{true}) = \pm 90°$. The deterioration of the CPV sensitivity is smaller for 360 km

and, with a minimum sensitivity of around 5.7σ for $\delta_{CP}(\text{true}) = \pm 90°$. For the 200 km baseline, the deterioration further reduces, with a minimum sensitivity of 6.1σ for all three benchmark choices, at $\delta_{CP}(\text{true}) = \pm 90°$. All in all, one sees that the degrading in CP sensitivity is not as
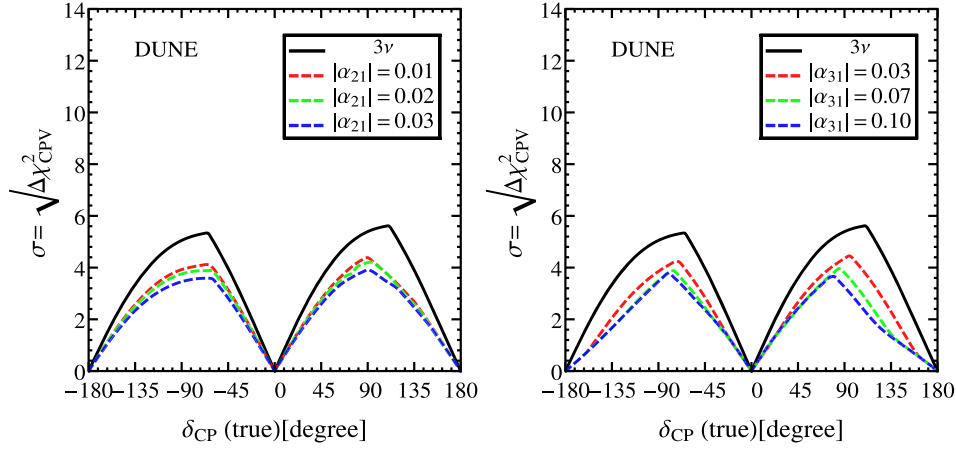
FIG. 6. CPV sensitivities at DUNE. Conventions and analysis procedure are the same as in Fig. 5; see its caption for details.

large as one might expect, showing the robustness of the oscillation picture with respect to unitarity violation. The best sensitivities to δ_{CP} and the nonunitary parameter $|\alpha_{21}|$ are achieved for a 200 km baseline.

We now turn to the right panels of Fig. 5. There, we repeated the same analysis for the nondiagonal parameter $|\alpha_{31}|$ and its associated CP phase, ϕ_{31}. The three benchmark choices considered for $|\alpha_{31}|$ are 0.03, 0.07, and 0.10.[5] In this case, one finds a mild deterioration of the CPV sensitivity in comparison to the unitary framework for all baselines, so the impact of $|\alpha_{31}|$ is not significant for 540 km, and negligible for 360 and 200 km baselines. This is due to the fact that $|\alpha_{31}|$ does not appear in the vacuum appearance probability, Eq. (16), and also because of the lower matter effects for ESSnuSB with respect to DUNE [7,64]. As expected, one finds a negligible impact on the CPV sensitivity arising from unitarity violation in this case. Note, however that this will not be the case for DUNE and, as a result, the combined analysis with ESSnuSB will be useful to recover the maximum CPV sensitivity in this case.

Next, in Fig. 6, we show the CPV sensitivities for DUNE. As before, the black solid lines in each panel correspond to the CPV sensitivity in the standard unitary framework, showing that DUNE can establish CPV discovery above 5σ for $\delta_{CP}(\text{true}) = \pm 90°$. The red, green, and blue dashed curves in the left panel represent the CPV discovery sensitivities in the NU framework corresponding to different values of $|\alpha_{21}|$: 0.01, 0.02, and 0.03, respectively. Similarly, in the right panel, these lines correspond to the CPV sensitivities for $|\alpha_{31}|$ equal to 0.03, 0.07, and 0.10. The simulation method followed in both the panels is the same as for Fig. 5. From the left panel, we see that the CPV sensitivity in the presence of NU is degraded with respect to the unitary framework, according to the value of $|\alpha_{21}|$. As a

result, for the maximal values of $\delta_{CP}(\text{true})$ one can only ensure a minimum CPV sensitivity of 3.6σ. Similarly, from the right panel, we can see that the CPV sensitivity decreases with increasing $|\alpha_{31}|$ with a minimum sensitivity of 3.6σ for $\delta_{CP}(\text{true}) = \pm 90°$.

Comparing Figs. 5 and 6, one sees that, for the conventional unitary scenario, the CPV sensitivity of ESSnuSB is better than that of DUNE. Also the deterioration due to NU effects is smaller than for DUNE, where the matter effect is large. Hence, in this case, ESSnuSB will play a complementary role to DUNE in achieving a robust CP violation sensitivity in the presence of nonunitarity.

So far we have analyzed the effect of the nondiagonal NU parameters on the CPV sensitivity of the experimental setups under consideration. Now we will investigate the role of the diagonal nonunitary parameters, α_{11}, α_{22}, and α_{33}. The corresponding CPV sensitivities in this case for ESSnuSB and DUNE are shown in the four panels of Fig. 7. The results for the standard unitary case (solid black line) for both the ESSnuSB and DUNE have been already described in Figs. 5 and 6. The red, green, and blue dashed lines in each panel correspond to the CPV sensitivities for fixed values of $\alpha_{11} = 0.94$, $\alpha_{22} = 0.99$, and $\alpha_{33} = 0.90$, respectively, in the data as well as in the theory. The procedure we have followed for this analysis is slightly different from what we have used for the nondiagonal parameters. In order to evaluate the CPV sensitivity in the NU framework for $\alpha_{11} = 0.94$, we have marginalized over α_{22}, $|\alpha_{21}|$, and ϕ_{21} within their allowed 3σ ranges. All other off-diagonal parameters are assumed to be zero, and we have also fixed $\alpha_{33} = 1$ in the data as well as in the theory. The analysis method for α_{22} is analogous to the previous one, where we have marginalized over α_{11}, $|\alpha_{21}|$, and ϕ_{21}. On the other hand for α_{33}, we marginalized over α_{11}, $|\alpha_{31}|$, and ϕ_{31}, fixing $\alpha_{22} = 1$.

One sees that ESSnuSB performs better than DUNE for the overall CPV discovery sensitivity. Of course, in all cases these sensitivities are degraded substantially with

---

[5]Note that, as in the previous case, the third value of $|\alpha_{31}|$ lies slightly outside the 3σ current limit, and is taken only for comparison.
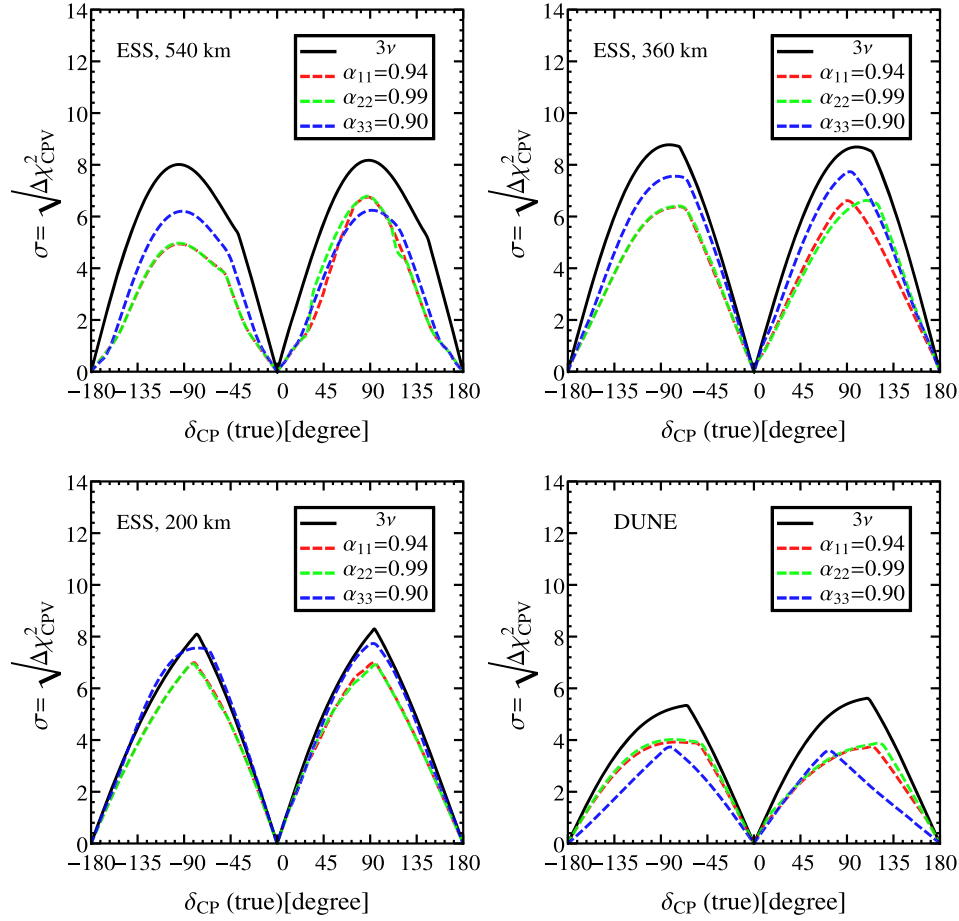
FIG. 7.   CPV sensitivities at ESSnuSB for the three baselines under consideration and for DUNE. The red, green, and blue dashed lines in each panel correspond to the CPV sensitivities for the fixed values of $\alpha_{11} = 0.94$, $\alpha_{22} = 0.99$, and $\alpha_{33} = 0.90$, respectively, in the data as well as in the theory. For simulation details, see the text.

respect to those of the unitary case. In fact, the CPV discovery for DUNE falls below 4σ for any value of δ_{CP}(true). As seen in Fig. 7 the best result is obtained for the 200 km baseline, followed by 360 km of ESSnuSB.

In short, the ESSnuSB will play a crucial role in securing a robust CPV discovery sensitivity in the presence of unitarity deviations close to the current upper bound.

C. *CP* reconstruction

In our simplest scenario there are two relevant *CP* phases, the standard three-neutrino Dirac phase δ_{CP} and the phase ϕ_{21} associated to nonunitarity.[6] One can therefore have four "*CP* conserving" cases, when either of them equals 0 or π. Likewise, four cases in which one has "maximal" *CP* violation, defined by having the modulus of any of them equal to $\pi/2$. In this section, we discuss how

---

[6]Note that $|\alpha_{31}|$ and $|\alpha_{32}|$ enter only in the appearance neutrino probability through matter effects, strongly suppressing the sensitivity to the associated phases ϕ_{31} and ϕ_{32}.

well the European Spallation Source setups can reconstruct the standard *CP* phase δ_{CP} as well as the nonunitarity phase ϕ_{21} for a few selected benchmarks.

The results of our analysis are shown in Fig. 8. The upper two panels correspond to the two *CP* conserving cases $(0,0)$ and (π, π), and the lower two panels to the two *CP*-violating scenarios $(-\pi/2, -\pi/2)$ and $(\pi/2, \pi/2)$. The red, green, and cyan contours in each panel correspond to 540, 360, and 200 km baselines of the ESSnuSB experiment, respectively, whereas the orange contours represent the sensitivity expected in DUNE. All contours correspond to the 2σ level for 2 d.o.f. For this analysis, we have fixed $|\alpha_{21}| = 0.02$, which lies within the current 3σ allowed boundary. All the other off-diagonal NU parameters have been kept fixed to zero. We have marginalized over the mixing angles θ_{13} and θ_{23} and the atmospheric mass-squared splitting, Δm^2_{31}, as well as over the true and test values of the NU parameters α_{11}, α_{22}, α_{33} within their allowed ranges.

We have checked that the expected 1σ uncertainties on δ_{CP} (ϕ_{21}) for the *CP*-violating scenarios are 16° (100°) for
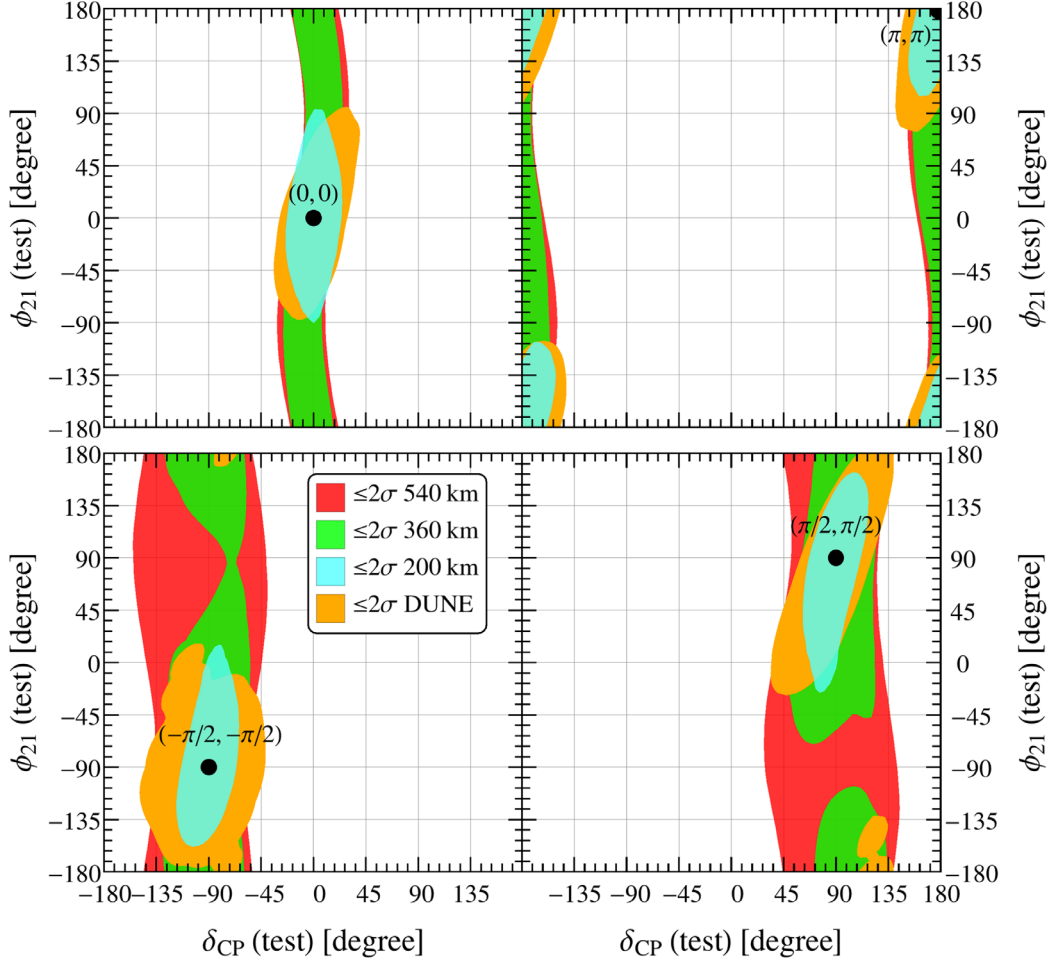
FIG. 8. *CP* reconstruction in the plane $[\delta_{CP}, \phi_{21}]$ (test) for different ESSnuSB baselines at 2σ level for 2 d.o.f. We have fixed $|\alpha_{21}| = 0.02$ and normal mass ordering in the data as well as in the theory. The red, green, and cyan contours correspond to 540, 360, 200 km baselines of the ESSnuSB experiment, respectively, whereas the orange contours denote the sensitivity expected in DUNE.

540 km, and 13° (70°) for 360 km. For the *CP*-conserving benchmarks, the uncertainties on δ_{CP} are 10° for 360 km, and 12° for 540 km respectively, whereas no sensitivity on ϕ_{21} is found for these two baselines. On the other hand, for the 200 km baseline, the typical 1σ level uncertainty on δ_{CP} (ϕ_{21}) is 10° (40°). One sees that the best performance would be obtained for the shortest baseline, 200 km. For comparison, we have also projected the sensitivity of the DUNE experiment in the same plot. For DUNE, the typical 1σ level uncertainty on the reconstructed *CP* phase δ_{CP} (ϕ_{21}) is 21° (45°).

In short, one can see that the δ_{CP} reconstruction capability of ESSnuSB does not get too much impaired by the presence of unitarity violation, while the sensitivity to the NU phase ϕ_{21} is competitive with that in DUNE and even better for 200 km baseline. Certainly, a future combined analysis of the actual results of these experiments would improve the standard and new *CP*–phase reconstruction sensitivities.

VI. SUMMARY AND OUTLOOK

Here we have explored the physics potential of the proposed European Spallation Source facility in the presence of nonunitarity of the lepton mixing matrix, as generally expected within the seesaw paradigm. We have also explored the DUNE physics potential in this framework as well as the combined result of both DUNE and ESSnuSB experiments. First, we presented in detail the theory framework of neutrino oscillations with effective nonunitary neutrino mixing, discussing in Fig. 1 the resulting neutrino and antineutrino appearance oscillation probabilities. Throughout the paper we have assumed normal neutrino mass ordering, and considered three reference baseline choices of 540, 360, and 200 km for the ESSnuSB setup. In Fig. 2 we have presented the sensitivity contours in the $(|\alpha_{21}|, \delta_{CP})$ plane. The promising results for the 200 km baseline were understood in terms of the expected $\nu_\mu \to \nu_e$ and $\bar{\nu}_\mu \to \bar{\nu}_e$ appearance event

spectra. These are given in Fig. 3 as a function of the reconstructed neutrino energy. We found encouraging ESSnuSB and DUNE sensitivities for the off-diagonal NU parameter $|\alpha_{21}|$, and the two diagonal NU parameters α_{11} and α_{22}, as seen in Fig. 4. One also sees how the combined analysis of DUNE and ESSnuSB can help with improving the sensitivity on the above mentioned NU parameters beyond the current 3σ bounds.[7]

More remarkable, perhaps, is the ESSnuSB CPV discovery potential, which is better than that of DUNE, as illustrated in Figs. 5, 6, and 7. One appreciates also a milder degrading of the ESSnuSB CP violation sensitivities with respect to the standard unitary mixing scenario in comparison with DUNE, where the effect is stronger. ESSnuSB would therefore contribute to establishing the robustness of CP determination against small departures from unitarity arising, say, from the seesaw mechanism. Finally, we have also obtained a promising CP reconstruction potential, both

for the standard CP phase of the three-neutrino paradigm, as well as for the phase associated to nonunitarity; see Fig. 8. Altogether, within the generalized nonunitary neutrino mixing framework, we have found that the proposed ESSnuSB facility is competitive and complementary to DUNE, not only for leptonic CP violation studies, but also for probing new physics parameters associated to unitarity violation.

ACKNOWLEDGMENTS

---

[7]The results we have obtained are also competitive with the sensitivity expected at future coherent elastic neutrino-nucleus scattering experiments [27].

[1] A. B. McDonald, Nobel lecture: The sudbury neutrino observatory: Observation of flavor change for solar neutrinos, Rev. Mod. Phys. **88**, 030502 (2016).

[2] T. Kajita, Nobel lecture: Discovery of atmospheric neutrino oscillations, Rev. Mod. Phys. **88**, 030501 (2016).

[3] P. F. de Salas, D. V. Forero, S. Gariazzo, P. Martínez-Miravé, O. Mena, C. A. Ternes, M. Tórtola, and J. W. F. Valle, 2020 global reassessment of the neutrino oscillation picture, J. High Energy Phys. 02 (**2021**) 071.

[4] P. F. De Salas, D. V. Forero, S. Gariazzo, P. Martínez-Miravé, O. Mena, C. A. Ternes, M. Tórtola, and J. W. F. Valle, Chi2 profiles from Valencia neutrino global fit, 10.5281/zenodo.4726908 (2021).

[5] R. Acciarri *et al.* (DUNE Collaboration), Long-baseline neutrino facility (LBNF) and deep underground neutrino experiment (DUNE), arXiv:1512.06148.

[6] O. Miranda, M. Tortola, and J. W. F. Valle, New Ambiguity in Probing CP Violation in Neutrino Oscillations, Phys. Rev. Lett. **117**, 061804 (2016).

[7] F. Escrihuela, D. V. Forero, O. G. Miranda, M. Tórtola, and J. W. F Valle, Probing CP violation with non-unitary mixing in long-baseline neutrino oscillation experiments: DUNE as a case study, New J. Phys. **19**, 093005 (2017).

[8] J. Schechter and J. W. F. Valle, Neutrino masses in $SU(2) \times U(1)$ theories, Phys. Rev. D **22**, 2227 (1980).

[9] J. Schechter and J. W. F. Valle, Neutrino oscillation thought experiment, Phys. Rev. D **23**, 1666 (1981).

[10] J. Schechter and J. W. F. Valle, Neutrino decay and spontaneous violation of lepton number, Phys. Rev. D **25**, 774 (1982).

[11] J. Bernabeu, A. Santamaria, J. Vidal, A. Mendez, and J. W. F. Valle, Lepton flavor nonconservation at high-energies in a superstring inspired Standard Model, Phys. Lett. B **187**, 303 (1987).

[12] G. Branco, M. Rebelo, and J. W. F. Valle, Leptonic CP violation with massless neutrinos, Phys. Lett. B **225**, 385 (1989).

[13] N. Rius and J. W. F. Valle, Leptonic CP violating asymmetries in Z^0 decays, Phys. Lett. B **246**, 249 (1990).

[14] M. Dittmar, A. Santamaria, M. Gonzalez-Garcia, and J. W. F. Valle, Production mechanisms and signatures of isosinglet neutral heavy leptons in Z^0 decays, Nucl. Phys. **B332**, 1 (1990).

[15] F. Deppisch and J. W. F. Valle, Enhanced lepton flavor violation in the supersymmetric inverse seesaw model, Phys. Rev. D **72**, 036001 (2005).

[16] F. Deppisch, T. Kosmas, and J. W. F. Valle, Enhanced $\mu^- - e^-$ conversion in nuclei in the inverse seesaw model, Nucl. Phys. **B752**, 80 (2006).

[17] R. Mohapatra and J. W. F. Valle, Neutrino mass and baryon number nonconservation in superstring models, Phys. Rev. D **34**, 1642 (1986).

[18] M. Gonzalez-Garcia and J. W. F. Valle, Fast decaying neutrinos and observable flavor violation in a new class of majoron models, Phys. Lett. B **216**, 360 (1989).

[19] E. K. Akhmedov, M. Lindner, E. Schnapka, and J. W. F. Valle, Left-right symmetry breaking in NJL approach, Phys. Lett. B **368,** 270 (1996).

[20] E. K. Akhmedov, M. Lindner, E. Schnapka, and J. W. F. Valle, Dynamical left-right symmetry breaking, Phys. Rev. D **53,** 2752 (1996).

[21] M. Malinsky, J. Romao, and J. W. F. Valle, Novel Supersymmetric SO(10) Seesaw Mechanism, Phys. Rev. Lett. **95,** 161801 (2005).

[22] S.-F. Ge, P. Pasquini, M. Tortola, and J. W. F. Valle, Measuring the leptonic CP phase in neutrino oscillations with nonunitary mixing, Phys. Rev. D **95,** 033005 (2017).

[23] D. Meloni, T. Ohlsson, W. Winter, and H. Zhang, Nonstandard interactions versus non-unitary lepton flavor mixing at a neutrino factory, J. High Energy Phys. 04 (2010) 041.

[24] M. Blennow, P. Coloma, E. Fernandez-Martinez, J. Hernandez-Garcia, and J. Lopez-Pavon, Non-unitarity, sterile neutrinos, and non-standard neutrino interactions, J. High Energy Phys. 04 (**2017**) 153.

[25] O. G. Miranda, P. Pasquini, M. Tórtola, and J. W. F. Valle, Exploring the potential of short-baseline physics at Fermilab, Phys. Rev. D **97,** 095026 (2018).

[26] C. Soumya and M. Rukmani, Non-unitary lepton mixing in an inverse seesaw and its impact on the physics potential of long-baseline experiments, J. Phys. G **45,** 095003 (2018).

[27] O. Miranda, D. K. Papoulias, O. Sanders, M. Tórtola, and J. W. F. Valle, Future CEvNS experiments as probes of lepton unitarity and light-sterile neutrinos, Phys. Rev. D **102,** 113014 (2020).

[28] P. Coloma, J. López-Pavón, S. Rosauro-Alcaraz, and S. Urrea, New physics from oscillations at the DUNE near detector, and the role of systematic uncertainties, J. High Energy Phys. 08 (2021) 065.

[29] S. K. Agarwalla, S. Das, A. Giarnetti, and D. Meloni, Model-independent constraints on non-unitary neutrino mixing from high-precision long-baseline experiments, J. High Energy Phys. 07 (**2022**) 121.

[30] P. Zyla et al. (Particle Data Group), Review of particle physics, Prog. Theor. Exp. Phys. **2020,** 083C01 (2020).

[31] W. Rodejohann and J. W. F. Valle, Symmetrical parametrizations of the lepton mixing matrix, Phys. Rev. D **84,** 073011 (2011).

[32] H. Hettmansperger, M. Lindner, and W. Rodejohann, Phenomenological consequences of sub-leading terms in see-saw formulas, J. High Energy Phys. 04 (2011) 123.

[33] F. J. Escrihuela, D. V. Forero, O. G. Miranda, M. Tortola, and J. W. F. Valle, On the description of nonunitary neutrino mixing, Phys. Rev. D **92,** 053009 (2015).

[34] D. V. Forero, C. Giunti, C. A. Ternes, and M. Tortola, Non-unitary neutrino mixing in short and long-baseline experiments, Phys. Rev. D **104,** 075030 (2021).

[35] M. D. Messier, Evidence for neutrino mass from observations of atmospheric neutrinos with Super-Kamiokande. Ph.D. thesis, Boston University, 1999.

[36] E. A. Paschos and J. Y. Yu, Neutrino interactions in oscillation experiments, Phys. Rev. D **65,** 033002 (2002).

[37] E. Baussan et al. (ESSnuSB Collaboration), A very intense neutrino super beam experiment for leptonic CP violation discovery based on the European spallation source linac, Nucl. Phys. **B885,** 127 (2014).

[38] M. Dracos (ESSν SB project Collaboration), The ESSνSB project for leptonic CP violation discovery based on the european spallation source linac, Nucl. Part. Phys. Proc. **273**–**275,** 1726 (2016).

[39] M. Dracos, The european spallation source neutrino super beam, arXiv:1803.10948.

[40] M. Dracos and T. Ekelof (ESSvSB Collaboration), Neutrino CP violation with the ESS neutrino Super Beam (ESSνSB), Proc. Sci., ICHEP2018 (**2019**) 524.

[41] Enrique Fernandez Martinez (private communication).

[42] L. Agostino, M. Buizza-Avanzini, M. Dracos, D. Duchesneau, M. Marafini, M. Mezzetto, L. Mosca, T. Patzak, A. Tonazzo, and N. Vassilopoulos (MEMPHYS Collaboration), Study of the performance of a large scale water-Cherenkov detector (MEMPHYS), J. Cosmol. Astropart. Phys. 01 (2013) 024.

[43] Luca Agostino (private communication).

[44] A. Alekou et al., Updated physics performance of the ESSnuSB experiment, Eur. Phys. J. C **81,** 1130 (2021).

[45] B. Abi et al. (DUNE Collaboration), Long-baseline neutrino oscillation physics potential of the DUNE experiment, Eur. Phys. J. C **80,** 978 (2020).

[46] B. Abi et al. (DUNE Collaboration), Experiment simulation configurations approximating DUNE TDR, arXiv:2103 .04797.

[47] T. Alion et al. (DUNE Collaboration), Experiment simulation configurations used in DUNE CDR, arXiv:1606.09550.

[48] P. Huber, M. Lindner, and W. Winter, Simulation of long-baseline neutrino oscillation experiments with GLoBES (General long baseline experiment simulator), Comput. Phys. Commun. **167,** 195 (2005).

[49] P. Huber, J. Kopp, M. Lindner, M. Rolinec, and W. Winter, New features in the simulation of neutrino oscillation experiments with GLoBES 3.0: General long baseline experiment simulator, Comput. Phys. Commun. **177,** 432 (2007).

[50] P. Huber, M. Lindner, and W. Winter, Superbeams versus neutrino factories, Nucl. Phys. **B645,** 3 (2002).

[51] J. Kopp, Sterile neutrinos and non-standard neutrino interactions in GLoBES, https://www.mpi-hd.mpg.de/ personalhomes/globes/tools/snu-1.0.pdf (2019).

[52] A. M. Dziewonski and D. L. Anderson, Preliminary reference earth model, Phys. Earth Planet. Inter. **25,** 297 (1981).

[53] F. D. Stacey, *Physics of the Earth*, 2nd ed. (Wiley, New York, 1977).

[54] P. Astier et al. (NOMAD Collaboration), Final NOMAD results on $\nu_\mu \rightarrow \nu_\tau$ and $\nu_e \rightarrow \nu_\tau$ oscillations including a new search for tau-neutrino appearance using hadronic τ decays, Nucl. Phys. **B611,** 3 (2001).

[55] P. Astier et al. (NOMAD Collaboration), Search for $\nu_\mu \rightarrow \nu_e$ oscillations in the NOMAD experiment, Phys. Lett. B **570,** 19 (2003).

[56] E. Eskut et al. (CHORUS Collaboration), The CHORUS experiment to search for $\nu_\mu \rightarrow \nu_\tau$ oscillation, Nucl. Instrum. Methods Phys. Res., Sect. A **401,** 7 (1997).

[57] E. Eskut et al. (CHORUS Collaboration), Final results on $\nu_\mu \rightarrow \nu_\tau$ oscillation from the CHORUS experiment, Nucl. Phys. **B793,** 326 (2008).

[58] K. Abe et al. (T2K Collaboration), Improved constraints on neutrino mixing from the T2K experiment with 3.13×10^{21} protons on target, Phys. Rev. D **103,** 112008 (2021).

[59] A. Himmel, Plenary Talk from Neutrino 2020, https://zenodo.org/record/3959581#.YYMH8Jujk-I.

[60] P. Adamson *et al.* (MINOS+Collaboration), Search for Sterile Neutrinos in MINOS and MINOS + using a Two-Detector Fit, Phys. Rev. Lett. **122**, 091803 (2019).

[61] D. Dutta and S. Roy, Non-unitarity at DUNE and T2HK with charged and neutral current measurements, J. Phys. G **48**, 045004 (2021).

[62] F. An *et al.* (JUNO Collaboration), Neutrino physics with JUNO, J. Phys. G **43**, 030401 (2016).

[63] S. K. Agarwalla, S. Choubey, and S. Prakash, Probing neutrino oscillation parameters using high power superbeam from ESS, J. High Energy Phys. 12 (2014) 020.

[64] B. Abi *et al.* (DUNE Collaboration), Prospects for beyond the standard model physics searches at the deep underground neutrino experiment, Eur. Phys. J. C **81**, 322 (2021).